

Ion Beam Analysis Of Silicon-Based Surfaces And Correlation With Surface Energy Measurements

Qian Xing^a, N. Herbots^a, M. Hart^a, J. D. Bradley^a, B. J. Wilkens^a, D. A. Sell^a, Clive H. Sell^b, Henry Mark Kwong Jr^b, R. J. Culbertson^a, S. D. Whaley^a

^aDepartment of Physics, Arizona State University, Tempe, AZ 85287-1504

^bAssociated Retina Consultants, 7600 N 15th Street, Suite 155, Phoenix, AZ 85020

Abstract. The water affinity of Si-based surfaces is quantified by contact angle measurement and surface free energy to explain hydrophobic or hydrophilic behavior of silicone, silicates, and silicon surfaces. Surface defects such as dangling bonds, surface free energy including Lewis acid-base and Lifshitz-van der Waals components are discussed. Water nucleation and condensation is further explained by surface topography. Tapping mode atomic force microscopy (TMAFM) provides statistical analysis of the topography of these Si-based surfaces. The correlation of the above two characteristics describes the behavior of water condensation at Si-based surfaces. Surface root mean square roughness increasing from several Å to several nm is found to provide nucleation sites that expedite water condensation visibly for silica and silicone. Hydrophilic surfaces have a condensation pattern that forms puddles of water while hydrophobic surfaces form water beads. Polymer adsorption on these surfaces alters the water affinity as well as the surface topography, and therefore controls condensation on Si-based surfaces including silicone intraocular lens (IOL). The polymer film is characterized by Rutherford backscattering spectrometry (RBS) in conjunction with 4.265 MeV ¹²C(α , α)¹²C, 3.045 MeV ¹⁶O(α , α)¹⁶O nuclear resonance scattering (NRS), and 2.8 MeV elastic recoil detection (ERD) of hydrogen for high resolution composition and areal density measurements. The areal density of hydroxypropyl methylcellulose (HPMC) film ranges from 10¹⁸ atom/cm² to 10¹⁹ atom/cm² gives the silica or silicone surface a roughness of several Å and a wavelength of 0.16 ± 0.02 μm, and prevents fogging by forming a complete wetting layer during water condensation.

Keywords: ERD, NRS, RBS, AFM, polymer film, silicone, silica, Si(100), contact angle, surface free energy, surface topography, intraocular implant.

PACS: 61.05.Np, 82.80.Yc, 68.37.Ps, 87.64.Dz, 68.55.am, 68.35.Md, 68.55.jd, 68.55.Nq, 82.30.Rs

INTRODUCTION

Water affinity and condensation behavior of surfaces are of interdisciplinary interest across physics, material science, engineering, and medical applications¹⁻⁴. Defects such as dangling bonds and contaminants render the Si(100) surface hydrophilic. One can attribute this behavior to the surface free energy and intermolecular interaction between water molecules and solid surfaces^{5,6}. Cleaning, etching, and passivation of crystalline Si result in a lower surface energy, leading to a hydrophobic behavior of the surface.

Contact angle and surface tension are used to quantify water affinity utilizing Young's equation combined with Van Oss theory,

$$\gamma_{SL} = \gamma_S - \gamma_L \cos \theta \quad (1)$$

$$\gamma = \gamma^{LW} + 2\sqrt{\gamma^+ \gamma^-} \quad (2)$$

the modified Young-Dupré equation thus becomes

$$(1 + \cos \theta) \gamma_L = 2(\sqrt{\gamma_S^{LW} \gamma_L^{LW}} + \sqrt{\gamma_S^+ \gamma_L^-} + \sqrt{\gamma_S^- \gamma_L^+}) \quad (3)$$

with γ_L = liquid's surface tension, γ_S = solid's surface tension, γ_{SL} = surface tension at solid-liquid interface, γ^+ and γ^- = Lewis acid-base component of surface tension, γ^{LW} = Lifshitz-van der Waals component of surface tension, θ = contact angle made at the liquid/solid interface⁷. Large surface tension components or surface free energy result in the contact angle being small and surface being hydrophilic, while small surface tension results in the surface being hydrophobic. Although quartz silica and silicone surface free energy measurements have been conducted elsewhere⁶, the fused quartz and medical silicone samples used in this paper need to be quantified and compared.

The surface topography is also known to affect the condensation/nucleation behavior of water. The Kelvin equation,

$$\ln\left(\frac{p}{p_e}\right) = \frac{2\gamma V_M}{rRT} \quad (4)$$

where p = actual vapor pressure, p_e = equilibrium vapor pressure, γ = surface tension of liquid, V_M = molar volume of liquid, r = radius of the droplet, R = gas constant, and T = temperature shows the fact that the curvature of the water droplet affects condensation behavior. With the surface being rough due to capillary type features and the water droplet curvature $\frac{1}{r}$ being small (implying “large” r), water nucleation and condensation becomes easier. Conversely, water droplets would be more difficult to nucleate and condense as the surface becomes smoother and water droplet curvature becomes larger. Thus a change in surface topography results in changing of the water condensation behavior. However, experimentally applying the above concept to the surface of silica, silicone, and HPMC polymer coated surfaces given surface roughness parameters in the nm to μm range needs to be investigated.

Medical issues such as water condensation at the liquid/air interface of intraocular implants during vitreoretinal surgery after cataract extraction and intraocular lens (IOL) implantation¹⁻³ provided the motivation for this study of Si-based surface water condensation behavior.

MATERIALS AND METHODS

Materials And Preparations

Numerous experiments were conducted to carry out this research. De-ionized (DI) water is of 2 M Ω cm resistivity unless otherwise noted. Fused silica wafers are from Medtronic, and were cleaned via ultrasound agitation for 10 minutes in DI water of 18 M Ω cm resistivity. The silicone lenses used were Bausch & Lomb HD-500 intraocular lens (IOL). HPMC (C₃₂H₆₀O₁₉) CAS-9004-25-3, was 86 kDa molecular weight from Sigma-Aldrich and is hydrated using DI water.

Both the silica wafers and the silicone lenses are coated with HPMC film at room temperature, soaked in water-hydrated HPMC for 2 hours at various concentrations (from 0.20% w.t. to 1.00% w.t), then air dried under class 10K ventilation hood for a minimum of 24 hours.

Contact Angle And Roughness Measurements

The Sessile drop method⁸ is used to conduct the contact angle measurement. The liquid droplets range in sizes from 0.4 μL ~ 5.0 μL and are delivered using a syringe with a 23 gauge cannula. The contact angle is measured using computer fitting techniques on the digital images. Both droplet size and contact angle are computed via computer processing.

Roughness and length-scale of roughness of surfaces were determined by tapping mode atomic force microscopy (TMAFM, Agilent). The AFM was operated in air with a silicon tip in AC mode. Gwyddion was the software used to produce images and roughness parameters: R_q = root mean square roughness, λ_a = average wavelength of the profile, and Δ_a = average absolute slope.

Rutherford Backscattering Spectroscopy

Areal density was used to analyze the HPMC film using He⁺ Rutherford backscattering spectrometry (RBS). RBS has been used to analyze polymer and substrate profiles including diffusion profiles, the aging process of organic photovoltaic cells, and polymers used for medical purposes⁹⁻¹¹. Energy loss of ions can be used to determine the film thickness¹². Both the energy loss due to the in-path of incident α particles and the out-path of the scattered α particles need to be considered. Since Si exists in the substrate only and not in the film, one can measure the energy shift of the Si edge to determine the energy loss,

$$\Delta E = kE_0 - E \quad (5)$$

with ΔE = energy loss, k = kinematic factor, E_0 = incident ion energy, E = ion energy at the detector. Therefore to determine the areal density of the film,

$$Nt = \frac{kE_0 - E}{k \frac{1}{|\cos \theta_1|} (\varepsilon_{E_0}) + \frac{1}{|\cos \theta_2|} (\varepsilon_{kE_0})} \quad (6)$$

where using Bragg's rule to compute the energy stopping factor,

$$\varepsilon_{C_{32}H_{60}O_{19}} \approx \frac{32\varepsilon_C + 60\varepsilon_H + 19\varepsilon_O}{32 + 60 + 19} \quad (7)$$

with θ_1 = incident angle to sample normal and θ_2 = detector angle to sample normal. ε = the stopping cross section of alpha particles in the HPMC. An incident angle of 0° (normal to the surface) was used for films prepared with of 0.33% - 1.00% w.t. HPMC in water, while 65° incident angle was chosen for films prepared with < 0.33% w.t. HPMC in water. The incident angles were chosen so that the silicon edge of

the RBS spectra would be exposed for thicker films, while being able to enhance the energy loss resolution for thinner films. Detector angle is 170° and incident energy is 2 MeV with the beam current ~ 20 nA.

HPMC consists of lighter C and O atoms which are typically difficult to detect on heavier substrates with a high degree of resolution. By implementing 4.265 MeV $^{12}\text{C}(\alpha, \alpha)^{12}\text{C}$ and 3.045 MeV $^{16}\text{O}(\alpha, \alpha)^{16}\text{O}$ nuclear resonance scattering (NRS), one can determine the carbon versus oxygen composition at high resolution near the surface. Again in these measurements, the incident beam is normal to the sample; detector angle is 170° , and beam current is ~ 20 nA.

The sample is separately measured for the height of the carbon and oxygen signals at 4.265 MeV and 3.045 MeV respectively. To maintain consistency, the Si signal is used to normalize all spectra,

$$\frac{N_C t}{N_O t} = \frac{\frac{\sigma_{Si}|_{E=C\text{-Resonance}} \cdot \frac{H_C}{H_{Si}}|_{E=C\text{-Resonance}}}{\sigma_C|_{E=C\text{-Resonance}}}}{\frac{\sigma_{Si}|_{E=O\text{-Resonance}} \cdot \frac{H_O}{H_{Si}}|_{E=O\text{-Resonance}}}{\sigma_O|_{E=O\text{-Resonance}}}} \quad (8)$$

with the subscripts of Si, O, and C representing silicon, oxygen, and carbon respectively, $\frac{H_C}{H_{Si}}$ and

$\frac{H_O}{H_{Si}}$ = normalized yield over Si signal, σ_C and σ_O =

scattering cross section at resonance, $N_C t$ and $N_O t$ = areal density of carbon and oxygen in HPMC film. The carbon and oxygen signal heights, respectively, were extracted from the RBS spectra by performing a linear fit to the background silicon signal and then subtracting the fitted background.

Elastic recoil detection (ERD) of the hydrogen atom is conducted to provide a comparative method to the above areal density measurement, as well as determining the hydrogen composition ratio. Incident α particles at 2.8 MeV with a 10.6 μm mylar filter at the detector are used. Projectile angle is 75° in reference to the sample normal and elastic recoil detector angle is 30° . Once again the beam current is kept at ~ 20 nA. RUMP simulation is then implemented to determine the areal density (Nt) of the HPMC film and the relative hydrogen composition compared to oxygen and carbon.

Ion beam damage in polymer films is a well known and impeding issue¹³. Therefore it was necessary to construct damage curves, which can then be used to extrapolate the effective non-damaged yield in the subsequent areal density measurement using regression modeling¹⁴.

Sample charging due to the ion beam incidence is observed for both silica wafer and silicone lens samples. Grounding with an aluminum foil wrapping with a 4 mm \sim 10 mm diameter hole minimizes the charging effect; enabling consistent, reproducible data collection. However, the charging effect still was significant enough to require an offset in terminal voltage to compensate for the required resonance energy; and hence this offset was introduced after adding the conductive wrapping. Resonance yield was not stable at the fixed carbon resonance of 4.265 MeV and oxygen resonance of 3.045 MeV. Therefore, the scattering yield was maximized around 4.265 MeV and 3.045 MeV by adjusting the offset due to the charging effect to obtain the resonance energy for collection of the spectra. The experiment was conducted in vacuum of 10^{-7} torr \sim 10^{-6} torr.

RESULTS AND DISCUSSION

Condensation Behavior Versus Surface Free Energy And Surface Topography

The contact angle and related surface free energy components for silica and silicone samples are shown in Table 1. Surface free energy of silica is greater than that of silicone, particularly the Lewis basic component γ^- . This results in silica's hydrophilic behavior versus silicone's hydrophobic behavior, which is shown by their respective contact angles.

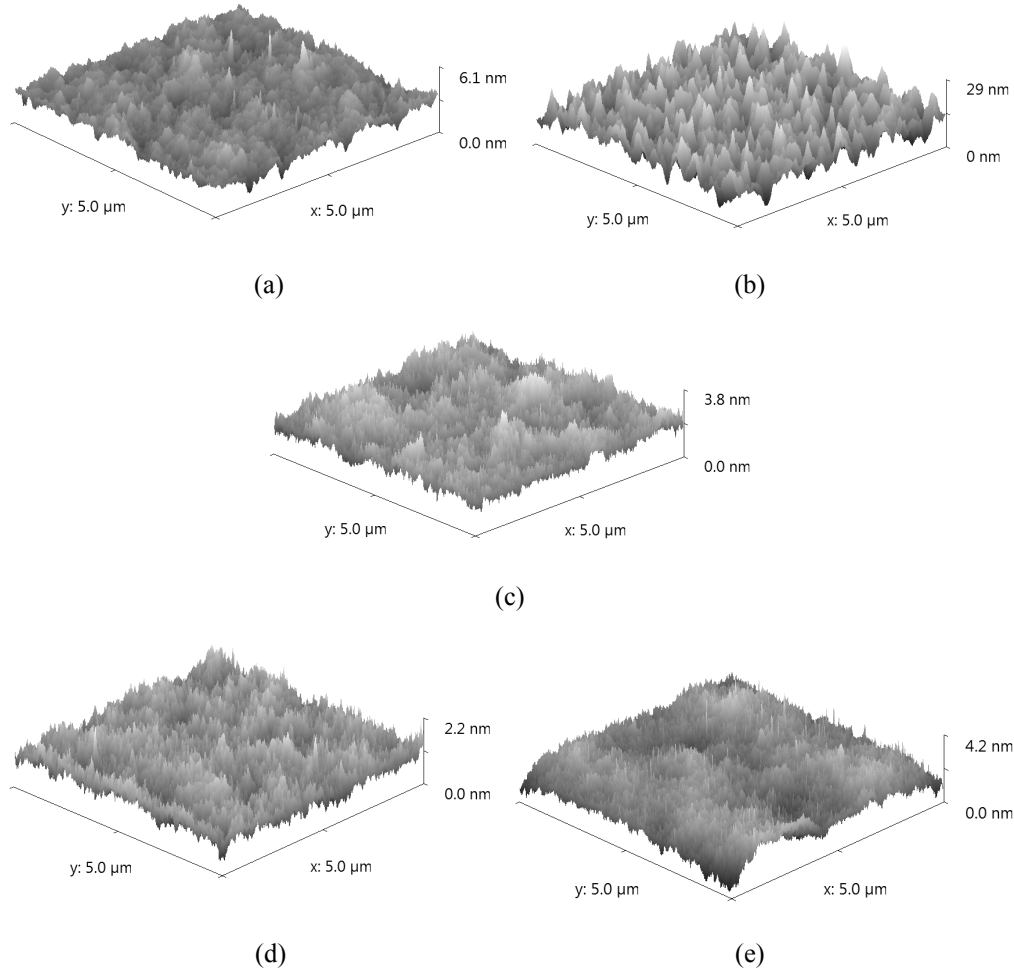
Surface topography images by TMAFM are shown in Figures 1a and 1b. Table 2 lists the roughness parameters of the respective samples. Notably, the roughness of the silicone is 9 times greater than that of the silica and the slope of features in silicone is about 7 times greater. However, the topographical wavelength of both samples is in the same range. Therefore, silicone provides more nano-scale capillary features.

TABLE 1. Surface Energies of Silicone and Silica Correspond to the Hydrophobic and Hydrophilic Behavior of the Respective Surfaces.

Type	γ^{LW} (mJ/m ²)	γ^+ (mJ/m ²)	γ^- (mJ/m ²)	Contact Angle with Water θ°
PDMS Silicone	19.4 ¹⁵	0.8 ¹⁵ (γ^{polar})		107.2 ¹⁵ 104.7 \pm 1.4 (from this work)
Silica	41.3 ¹⁶	2.21 ¹⁶	35.68 ¹⁶	30.77 (calculated using Equation (3)) 32.2 \pm 1.9 (from this work)

TABLE 2. Roughness Parameters via AFM.

Surface Type	R_q (nm)	λ_a (μm)	Δ_a
Silicone	3.7(2)	0.28(3)	0.067(4)
Quartz	0.42(5)	0.22(3)	0.0094(8)
HPMC 1% on Silicone	0.31(1)	0.16(1)	0.0098(4)
HPMC 1% on Silica	0.192(9)	0.16(2)	0.0064(7)
HPMC 0.2% on Silica	0.34(4)	0.16(2)	0.0110(7)

**FIGURE 1.** AFM 5 x 5 μm images of (a) silica, (b) silicone, (c) HPMC 1% on silicone (d) HPMC 1% on silica, and (e) HPMC 0.2% on silica.

From Tables 1 and 2 we can explain the differences in the condensation behavior that silicone and silica experience which further show how the morphology and water affinity affect condensation behavior. Silicone is much rougher than silica, and hence one can imagine that each peak-valley-peak as a capillary-like structure. This allows for almost immediate condensation as seen in Figure 2c. However, because the roughness effectively isolates each condensed water drop, the total condensation area remains finely fogged from a macroscopic view, as seen in Figure 2d. Since the surface free energy is relatively low

compared to the silica, the condensed water drops tend to form water “beads”.

The condensation behavior on the silica is quite different, as seen in Figures 2a and 2b. Because of its smoothness, it takes much longer than the silicone for water droplets to nucleate on its surface. However, once these droplets are nucleated, due to the high surface free energy, the resulting condensation then tends to coalesce faster than that on the silicone. As a result, instead of a fine mist like fog as seen on the silicone, the condensation rapidly takes on the form of “puddles” of water spaced over the silica.

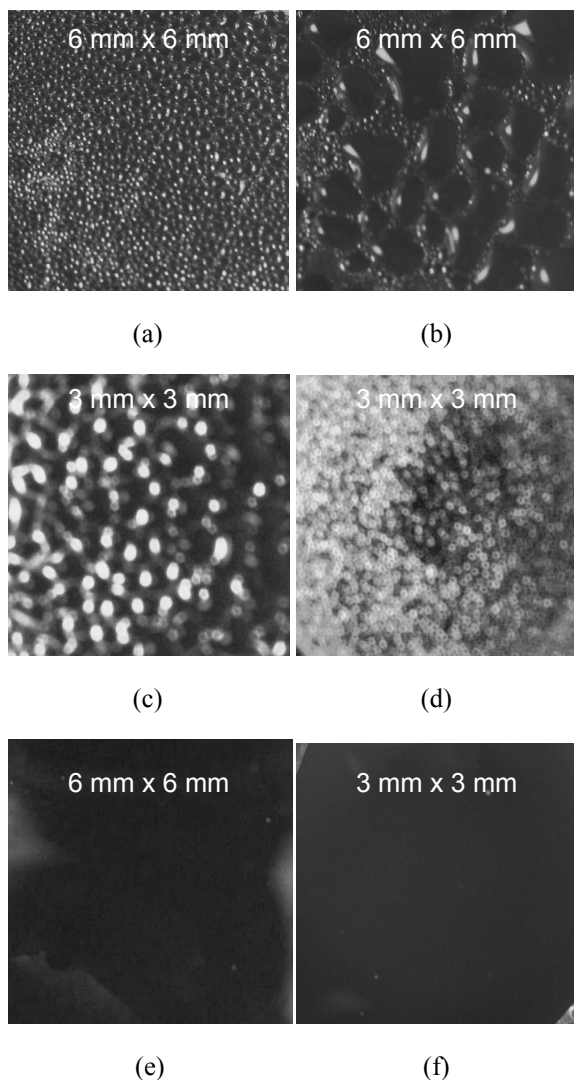


FIGURE 2. Condensation test. The water temperature is 70 °C. (a) 30 seconds after the silica is placed over the hot water. (b) 90 seconds after silica placement. The nucleated drops quickly coalesce into larger droplets. (c) 3 seconds after silicone is placed over the hot water. (d) 90 seconds after silicone placement. The nucleated drops tend to remain in place and coalescence is much slower than silica. (e) HPMC 1% coated silica over the hot water. (f) HPMC 1% coated silicone over the hot water. Complete wetting layer forms evenly.

HPMC polymer coating was used to alter the condensation behavior of silica and silicone. TMAFM was used to determine how the HPMC coating modified the surface topography of the respective silica and silicone substrate as shown in Figures 1c, 1d, and 1e. Roughness parameters in Table 2 demonstrate the wavelength was reduced significantly. HPMC is a water hydratable polymer which forms a water cage around its polymer chain via hydrogen bonding and has a high level of water affinity¹⁷. The

condensation behavior rapidly forms a complete wetting layer as shown in Figures 2e and 2f.

Polymer Film Composition And Areal Density Measurement

HPMC polymer film was characterized by areal density measurements via ion beam energy loss in conjunction with the respective damage curve extrapolation as shown in Figure 3. The HPMC areal density was obtained by measuring the energy shift as defined in Equation (6) above, with various incident α particle flux at 2 MeV to obtain the damage curve. Then the damage curve is fitted using exponential regression modeling. The concept and implementation of the damage curve was necessary since even small flux of α particle causes a reduction in polymer film areal density measurement. Using damage curves allows for the use of IBA as an analysis tool on films that are significantly damaged in the measurement process. More details regarding the damage curve will be reported elsewhere¹⁸. These results have demonstrated that HPMC film with an areal density ranging from 10^{18} atom/cm² ~ 10^{19} atom/cm² can effectively prevent fogging on the silica and silicone surfaces by forming a complete wetting layer to improve visual clarity. A film that is too thick will cause visual distortion, while too thin of a film may have a wide range of effects, from merely experiencing initial heavy fogging and then clearing, to not being effective at all due to complete fogging, or a combination of these effects.

The HPMC polymer film carbon and oxygen ratios near the film's surface is determined by 4.265 MeV $^{12}\text{C}(\alpha, \alpha)^{12}\text{C}$ and 3.045 MeV $^{16}\text{O}(\alpha, \alpha)^{16}\text{O}$ nuclear resonance scattering (NRS). Damage curves were used to compensate for the ion beam damage. Using the method specified in Equation (8) above, the resulting measured ratio gives,

$$\frac{N_C^{HPMC}}{N_O^{HPMC}} \approx 1.64 \pm 0.08 \quad (9)$$

which is in excellent agreement with the stoichiometric ratio of $\frac{C_{32}}{O_{19}} \approx 1.68$.

2.8 MeV elastic recoil detection (ERD) of hydrogen with RUMP simulation fitting is shown in Figure 4a. The areal density is 11600 (10^{15} atom/cm²), with increments of 100 (10^{15} atom/cm²) for each simulation step. The areal density measured by ERD is in excellent agreement with the areal density as extracted by the Si signal energy loss method, which gave a range of 11500 ~ 12500 (10^{15} atom/cm²) as an areal density in Figure 4b. The hydrogen composition to oxygen and carbon ratio was also determined to be

$N_C : N_O : N_H = 1.64 : 1.00 : 2.70$ with N_H step of 0.05, compared to the HPMC stoichiometric ratio of 1.68:1.00:3.16. The hydrogen content is 15% less than the bulk HPMC stoichiometric ratio would

suggest. This discrepancy is suspected to be from the loss of hydrogen atom due to the ion beam damage; however, it is not fully understood at this time and bears further investigation.

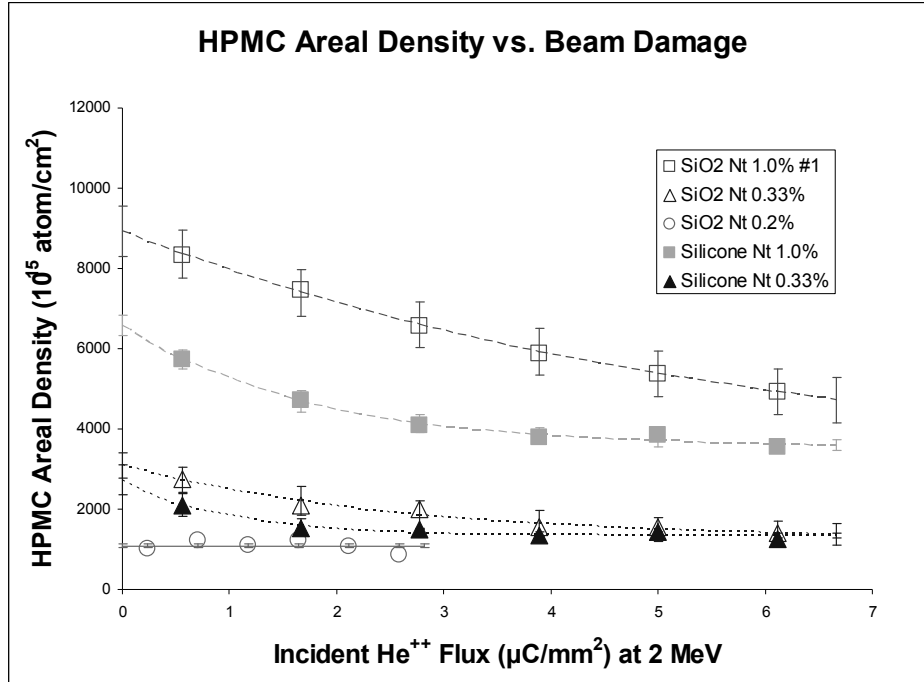


FIGURE 3. Damage curves conducted on SiO₂ (silica) and silicone substrates shown with polymer concentrations from 0.2% to 1.0%.

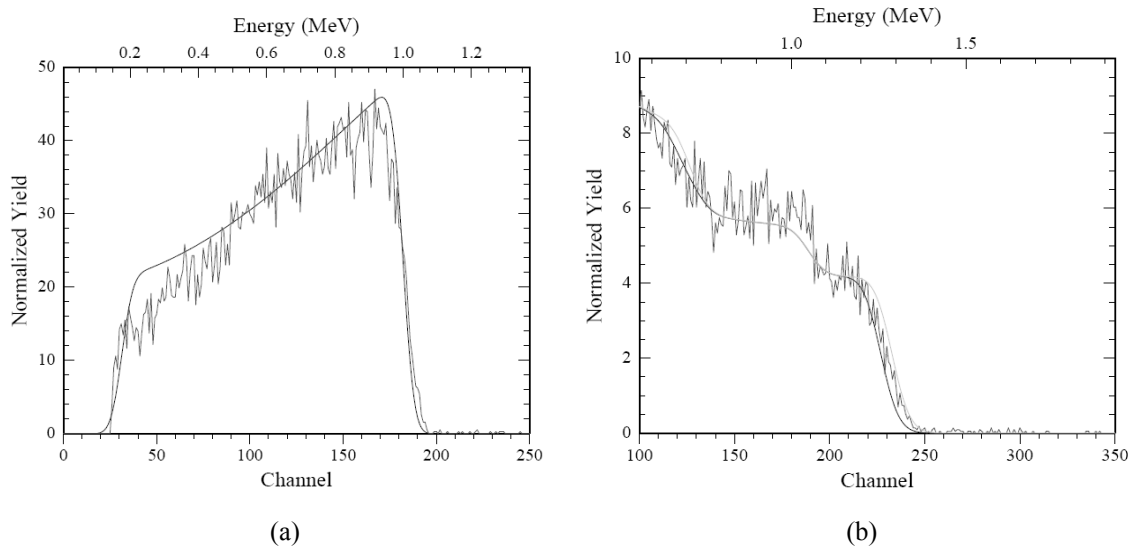


FIGURE 4. (a) ERD of HPMC film on silica substrate, with RUMP simulation. Simulation gives an areal density of 1.16×10^{19} atom/cm². (b) RUMP simulation executed twice on RBS spectrum of same HPMC film as in Figure 4a; areal density of simulation 1 (upper curve) = 1.15×10^{19} atom/cm², areal density of simulation 2 = 1.25×10^{19} atom/cm².

CONCLUSIONS

Characterization of a solid surface's water affinity via contact angle measurement using the Sessile Drop method, coupled with surface analysis using TMAFM, help explain the behavior of water condensation during liquid nucleation and condensation. Polymer adsorption on solid surfaces alters the water affinity, as well as the topography of the surface. Characterization of the polymer modified surface via IBA and TMAFM is correlated to the resulting change in behavior of water condensation and formation of wetting layer on the HPMC polymer surface.

The development of the damage curve was essential in enabling the use of IBA as a tool to characterize HPMC polymer, and allows for the compensation of the damage which the HPMC experiences during the IBA process. NRS and ERD, in combination with standard RBS, enable for the high resolution areal density measurement and composition determination of the HPMC film. TMAFM, along with the determination of surface free energy via the Sessile Drop method open up a new methodology to characterize and explain surface interactions in terms of surface free energy and surface topography.

Characteristics of the surface and the polymer film have been successfully quantified in this work. However, the condensation pattern is still qualitative in nature. Future work will involve quantifying this condensation pattern and relating it to surface characteristics, thus creating a truly predictive model for water condensation.

REFERENCES

1. R. Porter, *Ophthalmology*, 107 (4), 778-782 (2000).
2. Y. Yuriko, *Japanese Journal of Ophthalmic Surgery*, 18 (3), 383-386 (2005).
3. T. H. Levin, A New, Simple Technique to Prevent Water Condensation on Intraocular Lenses During Vitrectomy. NASA Technical Reports Server, Jet Propulsion Laboratory, NASA (2001).
4. M. Bjorkqvist, J. Paski, J. Solonen, and V. P. Lehto, *IEEE Sensors Journal*, 6 (3), 542-547 (2006).
5. H. Gouin, *J. Phys. Chem. B*, 102 (7), 1212-1218 (1998).
6. A. Carre, *J. Adhesion Sci. Technol.*, 21 (10), 961-981 (2007).
7. R. S. Faibish, *J. Colloid and Interface Sci.*, 256, 341-350 (2002).
8. E. Rame, *J. Colloid and Interface Sci.*, 185 (1), 245-251 (1997).
9. P. J. Mills, P. F. Green, C. J. Palmstrom, J. W. Mayer, and E. J. Kramer, *Appl. Phys. Lett.*, 45 (9), 957-959 (1984).
10. R. de Bettignies, J. Leroy, M. Firon, C. Sentein, S. Bailly and S. Guillerez, "Ageing Process in Organic Photovoltaic Solar Cell: Accelerated Lifetime and RBS Measurements", *European Conference on Hybrid and Organic Solar Cells* (2006).
11. M. Parizek, N. Kasalkova, L. Bacakova, P. Slepicka, V. Lisa, M. Blazkova, and V. Svorcik, *Int. J. Mol. Sci.*, 10, 4352-4374 (2009).
12. J. W. Mayer and E. Rimini, *Ion Beam Handbook for Material Analysis*, Academic Press, New York (1977).
13. M. P. de Jong, L. J. van IJzendoorn, and M. J. A. de Voigt, *Nucl. Instr. And Meth. In Phys. Research B.*, 161, 207-210 (2000).
14. J. M. Shaw, N. Herbots, Q. B. Hurst, D. Bradley, R. J. Culbertson, V. Atluri, and K. T. Queeney, *J. Appl. Phys.*, 100, 104109 (2006).
15. Diversified Enterprises, *Critical Surface Tension and Contact Angle with Water for Various Polymers* (2009).
16. A. Zdziennicka, *J. of Colloid and Interface Science*, 340, 243-248 (2009).
17. M. T. Levitt, *Proceedings of the National Academy of Sciences*, 104 (30), 12336-12340 (2007).
18. Q. Xing, M. Hart, N. X. Herbots, J. D. Bradley, R. J. Culbertson, D. A. Sell, C. H. Sell, H. M. Kwong, *Proceedings from the 17th International Conference on IBMM*, (to be published).